a length scale of 200 km with a reduction in V_s of only 2% (Fig. 3C, profile 3). By assigning different seismic velocities across the chemical interface, we find a V_s decrease of almost 3% in a distance of 100 km, with half of the decrease occurring as an abrupt jump (Fig. 3C, profiles 1 and 2). For low Rayleigh number cases (10^6), similar structures are found but the chemical layer is embedded in a broad thermal halo (Fig. 3C, profile 4). We have not been able to find a purely thermal plume that produces an interface sharp enough to give the *SKS* multipathing; we conclude that it is more likely that the interface has a chemical origin.

The inclination of the interface is also diagnostic of the dynamics. If the dense basal layer is stable, then the interface between the two layers is always tilted toward the center of the anomaly (Fig. 3B). We find that the interface becomes tilted away from the central anomaly only when the chemical layer is unstable, that is, when the thermal buoyancy is greater than the chemical. Moreover, the two sides of the rising diapir are generally not parallel (as the seismic observations of Africa suggest); both sides become tilted inward near the base of the mantle and outward near the top of the diapir (Fig. 3A).

Alternatively, the inclination could be caused by a large-scale mode of convection, including flow associated with plate motion. Over the past 100 million years (My), Africa has moved northeastward in a hot spot frame of reference (*15*). This motion is in the same overall direction as the tilting of the ALVS (*16*). Although previous models have been able to reproduce the tilt of the ALVS, a tilt that may be caused by the shear associated with the African plate (*17*), they typically display diffuse mantle structures inconsistent with the sharpness implied by *SKS* multipathing. This result motivates a second class of dynamic models with an imposed velocity boundary condition simulating the northeastward motion of Africa (Fig. 3, D through F). The thermo-chemical anomaly with sharp edges can be tilted, but we have been unable to find plumes with subparallel sides (Fig. 3E) or with widths comparable to their heights (Fig. 3D). When the coefficient of thermal expansion (α) decreases with depth, we are unable to match the shape of LVZ2. When α decreases with depth, thermo-chemical plumes are unstable in the mid-mantle but stable in the lowermost mantle, and the plumes give rise to tilts distinctly different from those observed. However, with a uniform α, we are able to reproduce the shape of the LVZ2 (Fig. 3F). The structure has sharp boundaries tilted over in the direction of plate motion, subparallel sides, and a width comparable to its height. The better fit of cases with apparently unrealistic α suggests that a physical process is absent from the dynamic models. However, models with sharp boundaries and outwardly tilting edges are always transient because the dense chemical layer is being actively entrained upward. The implications of this result are important for the thermal and chemical evolution of the mantle.

References and Notes

1. M. A. Richards, B. H. Hager, N. H. Sleep, *J. Geophys. Res.* **93**, 7690 (1988).
2. B. H. Hager, R. W. Clayton, M. A. Richards, R. P. Comer, A. M. Dziewonski, *Nature* **313**, 541 (1985).
3. C. Lithgow-Bertelloni, P. G. Silver, *Nature* **395**, 269 (1998).
4. M. Gurnis, J. M. Mitrovica, J. Ritsema, H.-J. van Heijst, *Geochem. Geophys. Geosys.* **1**, 1 (2000).
5. G. Masters, G. Laske, H. Bolton, A. Dziewonski, in *Earth's Deep Interior*, S. I. Karato, Ed. (American Geophysical Union, Washington, DC, 2000), pp. 63–87.
6. M. Ishii, J. Tromp, *Science* **285**, 1231 (1999).
7. M. Gurnis, *J. Geophys. Res.* **91**, 11407 (1986).
8. U. Hansen, D. A. Yuen, *Nature* **334**, 237 (1988).
9. P. J. Tackley, in *The Core-Mantle Boundary Region*, M. Gurnis, M. E. Wysession, E. Knittle, B. A. Buffett, Eds. (American Geophysical Union, Washington, DC, 1998), pp. 231–253.
10. See supporting online material on *Science* Online at www.sciencemag.org/cgi/content/full/296/5574/1850/DC1.
11. S. Ni, D. Helmberger, *Earth Planet. Sci.* **187**, 301 (2001).
12. _____, *J. Geophys. Res.*, in press.
13. G. F. Davies, M. Gurnis, *Geophys. Res. Lett.* **13**, 1517 (1986).
14. I. Sidorin, M. Gurnis, in *The Core-Mantle Boundary Region*, M. Gurnis, M. E. Wysession, E. Knittle, B. A. Buffett, Eds. (American Geophysical Union, Washington, DC, 1998), pp. 209–230.
15. R. D. Müller, J.-Y. Royer, L. A. Lawver, *Geology* **21**, 275 (1993).
16. J. Ritsema, H. J. van Heijst, J. H. Woodhouse, *Science* **286**, 1925 (1999).
17. C. P. Conrad, M. Gurnis, *Geochem. Geophys. Geosys.*, in preparation.
18. A. M. Dziewonski, D. L. Anderson, *Phys. Earth Planet. Inter.* **25**, 297 (1981).

19. Supported by NSF grants EAR-00001966 and EAR-9725808.

8 February 2002; accepted 5 April 2002

Polytype Distribution in Circumstellar Silicon Carbide

T. L. Daulton,[1,2*†] T. J. Bernatowicz,[3] R. S. Lewis,[4] S. Messenger,[3] F. J. Stadermann,[3] S. Amari[3]

The inferred crystallographic class of circumstellar silicon carbide based on astronomical infrared spectra is controversial. We have directly determined the polytype distribution of circumstellar SiC from transmission electron microscopy of presolar silicon carbide from the Murchison carbonaceous meteorite. Only two polytypes (of a possible several hundred) were observed: cubic 3C and hexagonal 2H silicon carbide and their intergrowths. We conclude that this structural simplicity is a direct consequence of the low pressures in circumstellar outflows and the corresponding low silicon carbide condensation temperatures.

Presolar grains (*1*) are identified by the presence of elements with anomalous isotopic compositions that are distinct from the average solar mixture in a manner that cannot be produced by in situ nuclear processes such as radioactive decay, mass fractionation, or cosmic ray–induced spallation reactions. The inference is that these grains are produced in stellar ejecta, and their isotopic compositions, in part, reflect nucleosynthetic processes that occurred in their stellar sources.

The two most abundant forms of presolar grains isolated from primitive meteorites are nanometer-sized diamond (*2*) and micrometer- to submicrometer-sized SiC (*3*). Both are ubiquitous in primitive chondritic meteorites at 300 to 1800 parts per million (ppm) (diamond) and 1 to 28 ppm (SiC) (*4*). Silicon carbide is particularly interesting because it is known to form hundreds of different polytype structures in the laboratory, and the formation of a particular polytype is sensitive to growth conditions. Astronomical evidence of SiC in dusty envelopes of carbon stars comes from a relatively broad 11.3-μm infrared (IR) feature (*5*). However, attempts to distinguish from such IR spectra (*6–9*) whether α-SiC or β-SiC (*10*) predominates in carbon stars remain controversial (*11–15*).

Isotopic analysis of Si, C, N, and other elements in individual presolar SiC grains by ion microprobe shows that 99% of the SiC originated from low-mass asymptotic giant branch (AGB) stars of variable metallicity (with a small fraction possibly from J stars), whereas the other 1% came from supernovae (*1*, *16*). Here, we assume that presolar SiC grains from primitive meteorites can be taken to be a representative sample of the grain contributions from all kinds of stellar

[1]Materials Science Division, Argonne National Laboratory, Argonne IL, 60439–4838, USA. [2]Marine Geosciences Division, Naval Research Laboratory, Stennis Space Center, MS 39529–5004, USA. [3]Laboratory for Space Sciences, Washington University, St. Louis, MO 63130–4899, USA. [4]Enrico Fermi Institute, University of Chicago, Chicago, IL 60637–1433, USA.

*Present address: Naval Research Laboratory.
†To whom correspondence should be addressed. E-mail: tdaulton@nrlssc.navy.mil

sources. If so, the laboratory determination of the crystallographic properties of a random selection of presolar SiC grains serves, to first order, as a direct measurement of the structure of SiC grains produced in the circumstellar outflows of low-mass AGB stars. Moreover, this determination is independent of astronomical observation.

Presolar SiC was isolated from fragments of the matrix of the Murchison (CM2) carbonaceous chondrite that did not contain any fusion crust by acid dissolution and was separated into nine size fractions: KJA to KJI (*17*) (Fig. 1). We determined the distribution of SiC polytypes in the KJB fraction, which contained the highest SiC abundance (1.91 ppm of the bulk meteorite, corresponding to over 1/3 the mass of SiC) and highest purity (97% SiC) of the nine fractions (*17*). Furthermore, KJB is a representative sample of the presolar SiC population because 70% of the Murchison SiC population lies within 0.3 to 0.7 μm, characteristic of 90% of the grains in KJB. Secondary ion mass spectrometry (SIMS) measurements of individual SiC grains in KJH, KJG, KJF (*18*), KJE (*19*), KJC (*20*), and KJB (*21*) indicate that >99% are presolar grains. For transmission electron microscopy (TEM) microcharacterization of SiC grains sufficiently large for subsequent isotopic analysis by nanometer-scale SIMS (NanoSIMS), the Murchison KJE (90% between 0.7 and 1.6 μm) size fraction was also studied.

Analysis of grains along one zone axis (*22*) by selected area electron diffraction (SAED) and high-resolution TEM (HR-TEM) lattice imaging demonstrates unambiguously that only two SiC polytypes were present in KJB: cubic 3C β-SiC (Fig. 2) and hexagonal 2H α-SiC (see Fig. 3) (*10*).

Intergrowths of these two polytypes were also observed. No other SiC polytypes were found among the 303 individual grains analyzed, with the exception of one 3C-2H SiC intergrowth grain containing many stacking faults and some short-range 4H order. Also, a small percentage of the heavily disordered grains were observed, which could not be identified as any polytype because they consisted of a random stacking of tetrahedral sheets.

Grains of 3C SiC were often multiply twinned with double diffraction present in SAED patterns, complicating polytype identification. One of the lowest energy interfaces in 3C SiC corresponds to twinning across {111} close-packed tetrahedral sheets. Twin boundaries in 3C SiC were predominantly of this type. Intergrowth grains contained variable proportions of 2H and 3C polytype order. As with 3C SiC single crystals, 3C SiC domains in intergrowth grains displayed a range of {111} twin microstructures and stacking fault densities. Each 3C SiC domain has four sets of <111> directions that can serve as an homoepitaxial growth interface to a 2H SiC domain, and nearly all intergrowth grains displayed one dominant 2H SiC orientation. Intergrowth grains often exhibited parallel 2H and 3C lamellae, but many contained only single large 2H and 3C domains. Electron diffraction and HR-TEM revealed no evidence of twinning in 2H SiC; however, stacking faults were observed.

Due to the large number of grains analyzed, it was impractical to identify their polytype other than from data along a single zone axis. Because of the finite tilt range of the TEM goniometer, a fraction of the randomly oriented grains will have no suitable zone axes (*22*) accessible. This fraction varies among SiC polytypes with distinctly different crystallographic symmetries (i.e., cubic, hexagonal, and rhombohedral). For example, there are 6 coplanar $<11\bar{2}0>$ hexagonal directions lying in the (0001) plane compared with 12 <011> cubic directions isometrically distributed in three dimensions. Consequently, the fraction of grains that can be identified varies with crystal system, biasing TEM-measured polytype distributions. Nonetheless, the true distribution can be estimated.

The relation between the actual number of

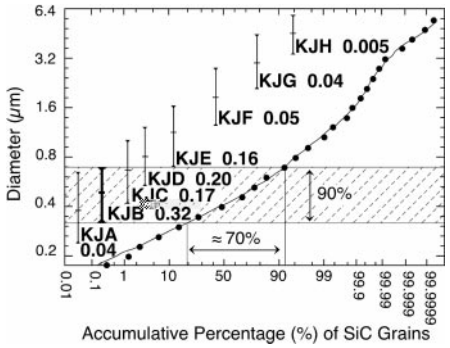

Fig. 1. Size distribution for Murchison SiC measured by scanning electron microscopy. Data points represent size bins differing by factors of $2^{1/5}$. The dominant size range (omitting the 5% tails in either end of the distribution) for each size fraction, KJA to KJH, is shown by vertical bars. The mean size for each fraction is shown by the horizontal bar. The relative mass within each size fraction is also indicated by the bold numbers. Ninety percent of KJB grains are in the size range corresponding to 70% of the Murchison population.

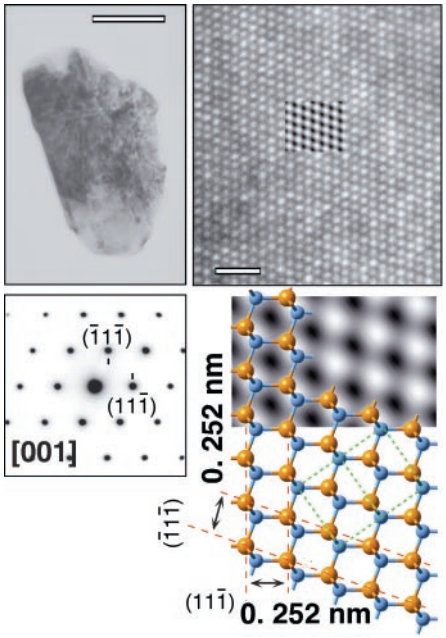

Fig. 2. Circumstellar 3C β-SiC from Murchison KJE. Bright-field image (**top**, **left**), SAED pattern (**bottom**, **left**), and HR-TEM lattice image (**top**, **right**) are shown together with an atomic model for the [011] zone axis superimposed on a simulated lattice image (**bottom**, **right**) using TEM defocus value to match the imaging conditions of the HR-TEM image. The tetrahedral stacking direction in the HR-TEM image and atomic model is along the horizontal. The red lines represent lattice planes and the green lines represent the unit cell. Scale bars: bright-field, 0.1 μm; HR-TEM, 1 nm.

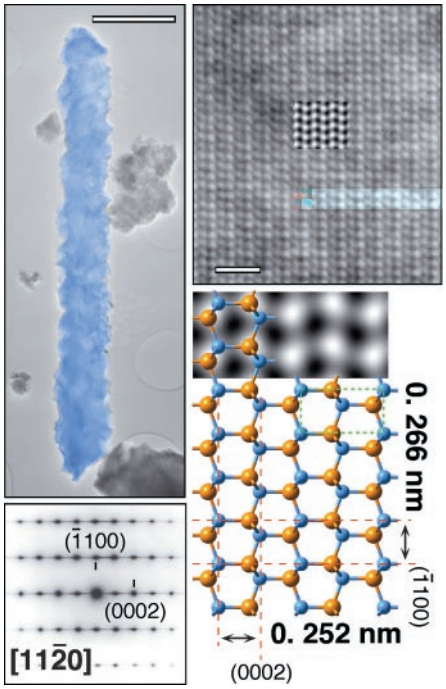

Fig. 3. Circumstellar 2H α-SiC from Murchison KJE. Bright-field image (**top**, **left**), SAED pattern (**bottom**, **left**), and HR-TEM lattice image (**top**, **right**) are shown together with an atomic model for the $[11\bar{2}0]$ zone axis superimposed on a simulated lattice image (**bottom**, **right**) using TEM defocus value to match the imaging conditions of the HR-TEM image. The tetrahedral stacking direction in the HR-TEM image and atomic model is along the horizontal. The red lines represent lattice planes and the green lines represent the unit cell. Scale bars: bright-field, 1 μm; HR-TEM, 1 nm. The grain displays long-range, well-ordered 2H stacking and has an atypical needle-like morphology. (Most presolar SiC grains are equant.)

grains (N) of a particular polytype and the number identified by TEM (N_T), can be described as

$$N = N_T \, \varepsilon_i^{-1} \quad (1)$$

where ε_i is the intrinsic fraction of randomly oriented crystals that have at least one suitable zone axis (*22*) within the TEM goniometer tilt limits ($\pm 45°$ and $\pm 30°$, solid angle $4\pi \times 0.1179$). The parameter ε_i was calculated by stereographic modeling of 10^8 random grain orientations. In addition to crystal symmetry, ε_i is dependent on twin and polytype intergrowth microstructure (*23*).

The KJB separate has a large number of SiC grains with 2H structure ($18.94 \pm 4.10\%$) as both 3C-intergrowths and single crystals (Table 1). Bulk and individual isotopic data (*18–21*), together with the abundance of these 2H SiC grains, suggest their circumstellar origin. Furthermore, isotopic analysis of an individual TEM-characterized 2H α-SiC from Murchison KJE (Fig. 3) by NanoSIMS (Fig. 4) directly establishes the grain as presolar (mean, $^{12}C/^{13}C = 65$, $^{14}N/^{15}N = 575$; terrestrial values are 89 and 269, respectively), consistent with mainstream SiC formed around low-mass AGB carbon stars. Therefore, circumstellar SiC unambiguously occurs as 2H α-SiC in addition to 3C β-SiC. Furthermore, the 2H SiC abundance and mainstream isotopic composition indicate that it is a relatively common grain type.

We propose that the polytype distribution of Murchison KJB SiC reflects original growth abundances as opposed to postgrowth thermal transformation products. Appreciable transformation of 2H → 3C and 3C → 6H requires at least 1673 to 1773 K and 1973 K, respectively (*24–26*). In comparison, experimental studies of volatization kinetics predict SiC grains (diameter ≤1 μm) would be destroyed by nebular gases ≥1200 K in less than 1000 years (*27*). Furthermore, the P3 presolar noble gas abundances in meteorites of metamorphic class CV3 imply the constituents of the meteorite, before and after accretion, experienced a thermal history approximately <870 K (*28*). Murchison has a lower metamorphic grade (CM2) and must have experienced lower temperatures. Although 6H SiC can also form directly by condensation, the fact that we identified no intergrowths (or single crystals) of the 6H polytype in presolar SiC supports the proposition that the population does not contain thermal transformation products.

The occurrence of the 3C and 2H SiC polytypes (and their intergrowths) as predominant in presolar SiC can be understood in terms of thermochemical equilibrium calculations (*29*, *30*). These predict that SiC condenses at ≤1633 K for any C/O ≥ 1.05 at pressures (<100 dyne/cm^2) believed to be present in carbon star outflows (*29*, *30*). Temperatures at which 2H SiC is known to grow and remain stable (~1473 to 1723 K) fall within this range (*24–26*, *31*, *32*). In condensation experiments that synthesize 2H SiC, formation of predominantly 3C SiC is observed at approximately >1700 K (*31*). A range of formation temperatures is reported in the literature for the different SiC polytypes. However, a phase diagram of polytype formation cannot be readily deduced from these studies because different processes are used to synthesize SiC and many experimental parameters vary. The most pertinent data are found in studies that examine the relative temperature dependence of several polytypes synthesized by a given process in which only a few experimental parameters are varied. A detailed review of the available literature on such studies indicates that all higher order SiC polytypes form at temperatures greater than that of 3C SiC under similar conditions for a given vapor condensation process (*33*). This explains why only two (2H and 3C) out of >250 possible polytypes are observed in circumstellar SiC.

The hypothesis suggested is that, close to carbon stars, photon and particle irradiation as well as temperatures are sufficiently high to prevent nascent nucleating clusters from reaching critical size for sustained growth. At radii in carbon star atmospheres, where irradiation and temperatures are sufficiently low, the highest temperature condensates, such as graphite and TiC, can form (*30*). At larger radii, the highest temperature SiC polytype observed, 3C, can condense. At still larger radii, in expanded cooler gas regions, the lower temperature 2H SiC can form. Thus, we infer that intergrowth grains probably formed at radii intermediate to the regions of predominantly 3C and 2H SiC formation. In particular, 2H SiC heteroepitaxial growth could occur on preexisting 3C SiC grains that were formed at smaller radii and transported by radiation pressure to cooler regions at larger radii.

Table 1. Murchison KJB SiC polytype distribution, based on TEM characterization of 303 grains, corresponding to >90% of the total grains examined. Excluded are those grains that, upon tilting, were found to be actually two grains randomly stuck together and those with no suitable zone axes within the goniometer tilt limits. The errors reflect the greater of sampling errors or the propagated uncertainties in ε_i for each grain. The uncertainties in ε_i for a grain result from uncertainties in determining the twin and intergrowth microstructure because not all 3C <111> twin planes, e.g., the inclined twin planes, are visible. In intergrowth grains, only those 2H domains associated with edge-on 3C <111> planes will be visible.

Grain type	Population (%)
3C	80.03 ± 2.38
2H/3C intergrowths	16.86 ± 4.07
2H	2.08 ± 0.52
Disordered	1.04 ± 0.33
All other polytypes (none observed)	<0.33

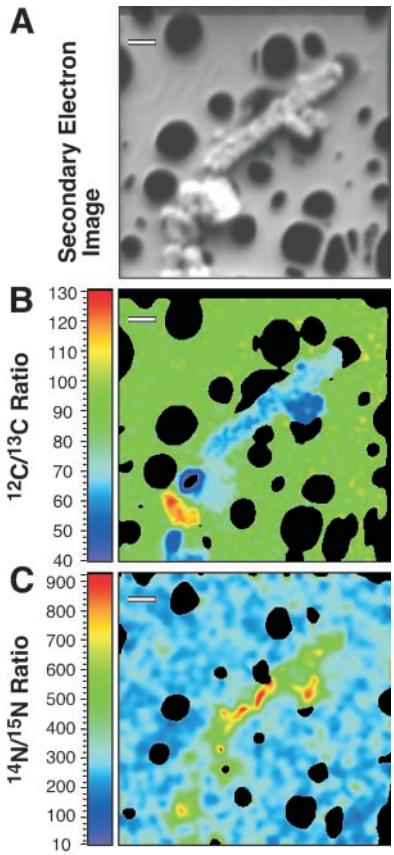

Fig. 4. NanoSIMS **(A)** secondary electron image and (**B** and **C**) isotopic ratio maps of $^{12}C/^{13}C$ and $^{14}N/^{15}N$, respectively, for the presolar 2H α-SiC shown in Fig. 3. Scale bar, 1 μm.

References and Notes

1. T. Bernatowicz, R. M. Walker, *Phys. Today* **50**, 26 (1997).
2. R. S. Lewis, T. Ming, J. F. Wacker, E. Anders, E. Steel, *Nature* **326**, 160 (1987).
3. T. Bernatowicz *et al.*, *Nature* **330**, 728 (1987).
4. G. R. Huss, R. S. Lewis, *Geochim. Cosmochim. Acta* **59**, 115 (1995).
5. R. Treffers, M. Cohen, *Astrophys. J.* **188**, 545 (1974).
6. A. Blanco, A. Borghesi, S. Fonti, V. Orofino, *Astron. Astrophys.* **283**, 561 (1994).
7. _____, *Astron. Astrophys.* **330**, 505 (1998).
8. M. A. T. Groenewegen, *Astron. Astrophys.* **293**, 463 (1995).
9. A. K. Speck, M. J. Barlow, C. J. Skinner, *Mon. Not. R. Astron. Soc.* **288**, 431 (1997).
10. In the notation described by L. S. Ramsdell [*Am. Mineral.* **32**, 64 (1947)], a polytype is denoted by the number of tetrahedral sheets in the unit cell followed by C, H, or R, representing crystal symmetry (i.e., cubic, hexagonal, or rhombohedral). The only cubic SiC polytype, 3C, is known as β-SiC, and all other SiC polytypes are known collectively as α-SiC.
11. R. Papoular, M. Cauchetier, S. Begin, G. LeCaer, *Astron. Astrophys.* **329**, 1035 (1998).
12. A. K. Speck, A. M. Hofmeister, M. J. Barlow, *Astrophy. J.* **513**, L87 (1999).
13. A. C. Andersen, *Astron. Astrophys.* **343**, 933 (1999).
14. H. Mutschke, A. C. Andersen, D. Clément, T. Henning, G. Peiter, *Astron. Astrophys.* **345**, 187 (1999).
15. T. Henning, H. Mutschke, *Spectrochim. Acta A* **57**, 815 (2001).

16. P. Hoppe, U. Ott, in *Astrophysical Implications of the Laboratory Study of Presolar Materials*, Proceedings of the AIP Conference, St. Louis, MO, 31 October to 2 November, 1996, T. Bernatowicz, E. Zinner, Eds. (American Institute of Physics Press, Springer-Verlag, New York, 1997), vol. 402, pp. 27–58.
17. S. Amari, R. S. Lewis, E. Anders, *Geochim. Cosmochim. Acta* **58**, 559 (1994).
18. P. Hoppe, S. Amari, E. Zinner, T. Ireland, R. S. Lewis, *Astrophys. J.* **430**, 870 (1994).
19. P. Hoppe, R. Strebel, P. Eberhardt, S. Amari, R. S. Lewis, *Geochim. Cosmochim. Acta* **60**, 883 (1996).
20. P. Hoppe, T. Kocher, P. Eberhardt, S. Amari, R. S. Lewis, *Meteorit. Planet. Sci.* **33**, A71 (1998).
21. E. Zinner, *Meteorit. Planet. Sci.* **36**, A231 (2001).
22. By "one zone axis," we mean a low-index zone axis perpendicular to the stacking direction of tetrahedral close-packed sheets (e.g., cubic <011> and hexagonal <11$\bar{2}$0>).
23. The presence of 3C {111} twin boundaries in a SiC grain increases the number of unique <011> orientations. The presence of several 2H domains, orientationally related to different 3C {111} planes in a SiC intergrowth grain, increases the number of unique <11$\bar{2}$0> orientations.
24. P. Krishna, R. C. Marshall, C. E. Ryan, *J. Cryst. Growth* **8**, 129 (1971).
25. G. A. Bootsma, W. F. Knippenberg, G. Verspui, *J. Cryst. Growth* **8**, 341 (1971).
26. P. Krishna, R. C. Marshall, *J. Cryst. Growth* **9**, 319 (1971).
27. R. A. Mendybaev *et al.*, *Geochim. Cosmochim. Acta*, **66**, 661 (2002).
28. G. R. Huss, in *Astrophysical Implications of the Laboratory Study of Presolar Materials*, Proceedings of the AIP Conference, St. Louis, MO, 31 October to 2 November, 1996, T. Bernatowicz, E. Zinner, Eds. (American Institute of Physics Press, Springer-Verlag, New York, 1997), vol. 402, pp. 721–748.
29. C. M. Sharp, G. J. Wasserburg, *Geochim. Cosmochim. Acta* **59**, 1633 (1995).
30. K. Lodders, B. Fegley, *Meteoritics* **30**, 661 (1995).
31. L. Patrick, D. R. Hamilton, W. J. Choyke, *Phys. Rev.* **143**, 526 (1966).
32. M. A. Stan, M. O. Patton, J. D. Warner, J. W. Yang, P. Pirouz, *Appl. Phys. Lett.* **64**, 2667 (1994).
33. H. Matsunami, *Phys. B* **185**, 65 (1993).
34. We thank M. A. Kirk and L. E. Rehn (Argonne National Laboratory) for encouragement. This work was partially supported by DOE, Naval Research Laboratory, NASA, and NSF.

Supporting Online Material
www.sciencemag.org/cgi/content/full/296/5574/1852/DC1
SOM Text

21 February 2002; accepted 16 April 2002

Germline Stem Cells Anchored by Adherens Junctions in the *Drosophila* Ovary Niches

Xiaoqing Song, Chun-Hong Zhu, Chuong Doan, Ting Xie*

How stem cells are recruited to and maintained in their niches is crucial to understanding their regulation and use in regenerative medicine. Here, we demonstrate that DE-cadherin–mediated cell adhesion is required for anchoring germline stem cells (GSCs) in their niches in the *Drosophila* ovary. Two major components of this adhesion process, DE-cadherin and Armadillo/β-catenin, accumulate at high levels in the junctions between GSCs and cap cells, one of the niche components. Removal of these proteins from GSCs results in stem cell loss. Furthermore, DE-cadherin is required for recruiting GSCs to their niche. Our study demonstrates that anchorage of GSCs in their niche by DE-cadherin–mediated adhesion is important for stem cell maintenance and function.

Stem cells exist in many adult tissues and are responsible for generating differentiated cells that replace cells lost during an animal's lifetime (*1*–*3*). Understanding the molecular mechanisms controlling stem cell function in vivo is crucial to the future use of stem cells in regenerative medicine, as well as in understanding aging, tumor formation, and degenerative diseases (*4*–*6*). GSCs in the adult *Drosophila* ovary are an excellent system in which to study stem cells and niches in vivo at the cellular and molecular levels (*7*, *8*). At the tip of the germarium (Fig. 1A), located at the tip of each ovariole of an ovary, a niche exists for two or three GSCs whose progeny eventually develop into mature oocytes (*9*–*12*). GSCs can be reliably identified based on size, location, and the shape of their fusome. Stem cells contain fusomes (also known as spectrosomes) that are usually round but can be elongated in shape while transiently connected to their daughter cells after division (*13*, *14*). These stem cells directly contact cap cells and are close to two other somatic cell types: terminal filament cells and inner germarial sheath cells. Terminal filament cells and cap cells express the genes, *decapentaplegic* (*dpp*), *fs(1)Yb* (*Yb*), *piwi*, and *hedgehog* (*hh*), which are known to be important for GSC maintenance (*9*–*12*).

Cell adhesion mediated by DE-cadherin, a *Drosophila* classic cadherin encoded by the *shotgun* (*shg*), and Armadillo (Arm), the *Drosophila* β-catenin homolog, plays an important role between germ cells and follicle cells during oogenesis (*15*–*19*). To determine whether DE-cadherin–mediated cell adhesion is important for anchoring GSCs in their niches, we first examined the expression of DE-cadherin and Arm proteins in the germarium. The *hh-lacZ* line, in which the bacterial *lacZ* gene with a basal promoter is inserted into the *hh* gene, was used to identify cap cells and terminal filament cells (*20*). These germaria were also immunostained for Hu-li Tai Shao (Hts) and/or Vasa proteins, molecular markers for the fusomes and germline cells, respectively (*21*, *22*). DE-cadherin protein accumulated at high levels as a single band in the interfaces between cap cells and GSCs (Fig. 1B). With more detergent than used in the normal procedure (*23*), the DE-cadherin band separated into two bands just between cap cells and GSCs (Fig. 1C). DE-cadherin is a membrane-associated protein, which accumulates on the membranes of cap cells and GSCs. Arm and DE-cadherin colocalized in these sites (Fig. 1, D to F). Note that the distribution of these proteins was not uniform in the contact areas between GSCs and cap cells or between cap cells themselves. Instead, there were focal sites between the cells that were rich in DE-cadherin and Arm proteins (Fig. 1F), possibly representing adherens junctions. Consistent with this idea, typical adherens junctions were observed between cap cells and GSCs (Fig. 1G), suggesting that DE-cadherin–mediated cell adhesion between cap cells and GSCs in the form of adherens junctions may be involved in anchoring GSCs to cap cells.

To investigate whether DE-cadherin–mediated cell adhesion is essential for maintaining GSCs in their niche, we used FLP-mediated recombination of the FLP recombination target sequences (FRTs) (*24*, *25*) to produce marked GSCs that lack functional copies of either *shg* or *arm* (*23*). The marked GSCs were identified by their loss of expression of *lacZ* (*9*). To investigate whether the removal of DE-cadherin from GSCs disrupts its accumulation in the contact sites, we used the deletion allele of *shg*, shg^{R69}, to remove DE-cadherin proteins from GSCs in the adult ovary (*15*). With this allele, DE-cadherin accumulation diminished in the interfaces between GSCs and cap cells within 1 week (Fig. 2, A and B). Partial depletion was observed in some cases, which may be due to the persistence of the protein (Fig. 2A). In the germaria containing shg^{R69} GSCs, the accumulation of DE-cadherin was maintained between wild-type GSCs and cap cells.

To further determine the importance of DE-cadherin–mediated adhesion in maintaining GSCs in their niche, we used two *shg* alleles: the deletion allele (shg^{R69}) and a weak allele (shg^{10469}) (*15*). Consistent with the prediction that the adhesion is important for anchoring GSCs, mutant shg^{R69} GSCs were lost very quickly (with a half-life of 0.8 weeks), causing marked shg^{R69} GSCs to occur at a much lower frequency in germaria during the first week after

Stowers Institute for Medical Research, 1000 East 50th Street, Kansas City, MO 64110, USA.

*To whom correspondence should be addressed. E-mail: tgx@stowers-institute.org